Microscopic Simulation of Congested Traffic

Martin Treiber[1], Ansgar Hennecke[1], and Dirk Helbing[1,2]

[1] II. Institute of Theoretical Physics, University of Stuttgart, Pfaffenwaldring 57/III, 70550 Stuttgart, Germany
[2] Collegium Budapest – Institute for Advanced Study, H-1014 Hungary

Abstract. We present simulations of congested traffic in open systems with a new car-following model. The model parameters are all intuitive and can be easily calibrated. Microsimulations with identical vehicles on a single lane produce the same traffic states as recent macrosimulations of open systems with on-ramps, which also qualitatively agree with real traffic data. The phase diagram in the phase space spanned by the traffic flow and the bottleneck strength is nearly equivalent to the macroscopic phase diagram. In agreement with macroscopic models, we found hysteresis, coexistent states, and a small region of tristability. We simulated the process of obtaining time-averaged traffic data by "virtual detectors". While for identical vehicles, the resulting flow-density data do not look very realistic, microsimulations of heterogeneous (multi-species) traffic offer a natural explanation of the observed wide scattering of congested traffic data.

1 Introduction

For about fifty years, now, researchers model freeway traffic by means of continuous-in-time microscopic models (car-following models) [1]. Since then, a multitude of car-following models have been proposed, both for single-lane and multi-lane traffic including lane changes.

In the simplest case, the acceleration of an individual vehicle depends only on the distance to the vehicle in front. Well-known models of this type include the model of Newell [2], or the "optimal-velocity model" by Bando *et al.* [3]. To achieve a better anticipative driver behavior and to avoid collisions, the acceleration in other models depends also on the velocity and on the approaching rate to the front vehicle [4–6]. Besides these simple models intended for basic investigations, there are also highly complex "high-fidelity models" with plenty of parameters like the Wiedemann model [7] or MITSIM [8], which try to reproduce traffic as realistically as possible.

From a physics point of view, a microscopic traffic model should be as simple as possible. The parameters should be intuitive, easy to calibrate, and the corresponding values should be realistic. The collective dynamics should reproduce all observed localized and extended traffic states [9], including synchronized traffic and the wide scattering of congested traffic data [10]. Furthermore, the observed hysteresis effects [11,12], complex states [10,13], and the existence of self-organized quantities like the constant propagation velocity of stop-and-go waves or the outflow from a traffic jam [14] should

be reproduced. To be consistent with macroscopic models, a deterministic instability mechanism is favourable. Finally, the dynamics must not lead to vehicle collisions and the model should allow for a fast numerical simulation.

In this paper, we check some of these criteria for the recently proposed intelligent-driver model (IDM) [15]. In particular, we give microscopic implementations of bottleneck inhomogeneities and present the phase diagram of congested traffic states for open, inhomogeneous systems [16]. We show that, for identical vehicles, the collective dynamics is qualitatively the same as that resulting from macroscopic traffic models like the non-local, gaskinetic-based traffic model (GKT model) [17], or the Kerner-Konhäuser-Lee model (KKL model) [14,18]. Finally, we investigate heterogeneous traffic (composed of cars and trucks) and propose a natural explanation of the observed wide scattering of congested traffic data.

2 The Microscopic Intelligent-Driver Model (IDM)

The acceleration assumed in the IDM is a continuous function of the velocity v_α, the (netto) gap s_α, and the velocity difference (approaching rate) Δv_α of vehicle α to the leading vehicle

$$\dot{v}_\alpha = a^{(\alpha)} \left[1 - \left(\frac{v_\alpha}{v_0^{(\alpha)}} \right)^\delta - \left(\frac{s_\alpha^*(v_\alpha, \Delta v_\alpha)}{s_\alpha} \right)^2 \right] . \tag{1}$$

This expression is a superposition of the acceleration $a^{(\alpha)}[1-(v_\alpha/v_0^{(\alpha)})^\delta]$ on a free road, and a braking deceleration $-a^{(\alpha)}[s_\alpha^*(v_\alpha, \Delta v_\alpha)/s_\alpha]^2$, describing the interactions with other vehicles. The deceleration term depends on the ratio between the "desired gap" s_α^* and the actual gap s_α, where the desired gap

$$s_\alpha^*(v, \Delta v) = s_0^{(\alpha)} + s_1^{(\alpha)} \sqrt{\frac{v}{v_0^{(\alpha)}}} + T^\alpha v + \frac{v \Delta v}{2\sqrt{a^{(\alpha)} b^{(\alpha)}}} , \tag{2}$$

is dynamically varying with the velocity and the approaching rate, reflecting an intelligent driver behavior. The IDM parameters are the desired velocity v_0, safe time headway T, maximum acceleration a, comfortable deceleration b, acceleration exponent δ, and the jam distances s_0 and s_1. Furthermore, the vehicles have a finite length l, which, however, has no dynamical influence. In Sections 2 to 4, we will assume identical "cars", while in Sec. 5 we assume two different types, "cars" and "trucks", see Table 1. For better readability, we will drop the vehicle index α in the following discussion of the model.

Table 1. Model parameters of the IDM model used throughout this paper.

Type	v_0	T	a	b	s_0	s_1	l
Cars	120 km/h	1.2 s	0.8 m/s^2	1.25 m/s^2	1 m	10 m	5 m
Trucks	80 km/h	1.7 s	0.4 m/s^2	0.8 m/s^2	1 m	10 m	8 m

2.1 Equilibrium Traffic of Identical Vehicles

In equilibrium traffic ($\dot{v}_\alpha = 0$, $\Delta v_\alpha = 0$), drivers tend to keep a velocity-dependent equilibrium gap $s_\mathrm{e}(v_\alpha)$ to the front vehicle given by

$$s_\mathrm{e}(v) = s^*(v,0)\left[1-\left(\frac{v}{v_0}\right)^\delta\right]^{-\frac{1}{2}}. \tag{3}$$

In particular, the equilibrium gap of homogeneous *congested* traffic ($v \ll v_0$) is essentially equal to the desired gap, $s_\mathrm{e}(v) \approx s^*(v,0) = s_0 + s_1\sqrt{v/v_0} + vT$, i.e., it is composed of a (small) high-density contribution, and a contribution vT corresponding to a time headway T.

Solving Eq. (3) for the equilibrium velocity $v = v_\mathrm{e}$ leads to simple expressions only for $s_1 = 0$ and $\delta = 1$, $\delta = 2$, or $\delta \to \infty$. In particular, the equilibium velocity for the special case $\delta = 1$ and $s_0 = s_1 = 0$ is

$$v_\mathrm{e}(s) = \frac{s^2}{2v_0T^2}\left(-1+\sqrt{1+\frac{4T^2v_0^2}{s^2}}\right). \tag{4}$$

Macroscopically, homogeneous traffic consisting of identical vehicles can be characterized by the equilibrium traffic flow $Q_\mathrm{e}(\rho) = \rho V_\mathrm{e}(\rho)$ (vehicles per hour and lane) as a function of the traffic density ρ (vehicles per km and lane). For $\delta = 1$ and $s_0 = s_1 = 0$, this "fundamental diagram" follows from Eq. (4) together with the micro-macro relation between gap and density,

$$s = 1/\rho - l = 1/\rho - 1/\rho_\mathrm{max}. \tag{5}$$

The result is identical with the equilibrium velocity of the GKT model, if the GKT parameter ΔA is set to zero, (cf. Eq. (23) in Ref. [17]), which is a necessary condition for a micro-macro correspondence. Figure 1 (a) shows that the acceleration coefficient δ influences the transition region between the free and congested regimes. For $\delta \to \infty$ and $s_1 = 0$, the fundamental diagram $Q_\mathrm{e}(\rho) = \min(v_0\rho, [1-\rho(l+s_0)]/T)$ becomes triangular-shaped. For decreasing δ, it becomes smoother and smoother.

2.2 Dynamic Single-Vehicle Properties

Figures 1(b) and 1(c) show how the parameters a and b determine the acceleration and braking behavior of single vehicles. At $t = 0$, one vehicle starts with

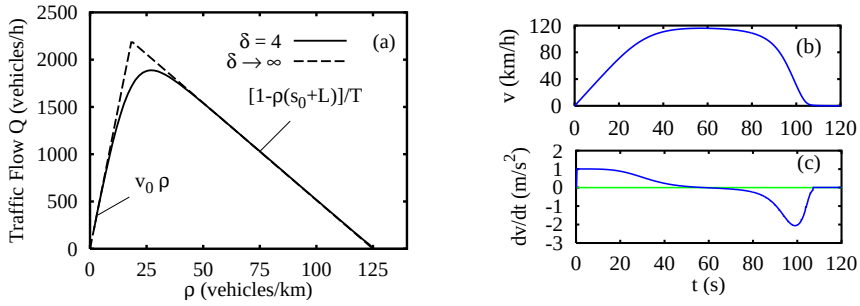

Fig. 1. (a) Equilibrium flow-density diagram of identical IDM vehicles with variable acceleration exponent δ and the "car" parameters of Table 1 otherwise. (b), (c) Temporal evolution of the velocity and acceleration of a single vehicle approaching a standing obstacle, which is reached after $t = 106$ s (cf. main text). The IDM parameters are $a = 1$ m/s^2, $b = 2$ m/s^2, and the "car" parameters of Table 1 otherwise.

zero velocity and 2.5 km of free road ahead. Initially, it accelerates with a and approaches smoothly the desired velocity v_0. At $x = 2.5$ km, we assume a standing obstacle, e.g., the end of a traffic jam. When approaching the obstacle, the model mimics "intelligent" drivers who anticipate necessary braking decelerations and brake so as not to exceed the comfortable deceleration b in normal situations [15].

2.3 Collective Behavior and Stability Diagram

Although we are interested in realistic *open* systems, it turned out that many features can be explained in terms of the stability behavior in a *closed* system. Figure 2(a) shows the stability diagram of homogeneous traffic on a circular road. The control parameter is the homogeneous density $\overline{\rho}$. We applied both a very small and a large localized perturbation to check for linear and nonlinear stability, and plotted the resulting minimum ($\rho_{\rm out}$) and maximum ($\rho_{\rm jam}$) densities after a stationary situation was reached. The resulting diagram is very similar to that of the macroscopic KKL and GKT models [14,17]. In particular, it displays the following realistic features: (i) Traffic is stable for very low and high densities, but unstable for intermediate densities. (ii) There is a density range $\rho_{\rm c1} \le \overline{\rho} \le \rho_{\rm c2}$ of metastability, i.e., only perturbations of sufficiently large amplitudes grow, while smaller perturbations disappear. Note that, for most IDM parameter sets, there is no second metastable range at higher densities, in contrast to the GKT and KKL models. (iii) The density inside of traffic jams and the associated flow $Q_{\rm jam} = Q_{\rm e}(\rho_{\rm jam})$, cf. Fig. 2(b), do not depend on $\overline{\rho}$. As further "traffic constants", at least in the density range 20 veh./km $\le \overline{\rho} \le$ 40 veh./km, we observe a constant outflow $Q_{\rm out} = Q_{\rm e}(\rho_{\rm out})$ and propagation velocity $v_{\rm g} = (Q_{\rm out} - Q_{\rm jam})/(\rho_{\rm out} - \rho_{\rm jam}) \approx -15$ km/h of

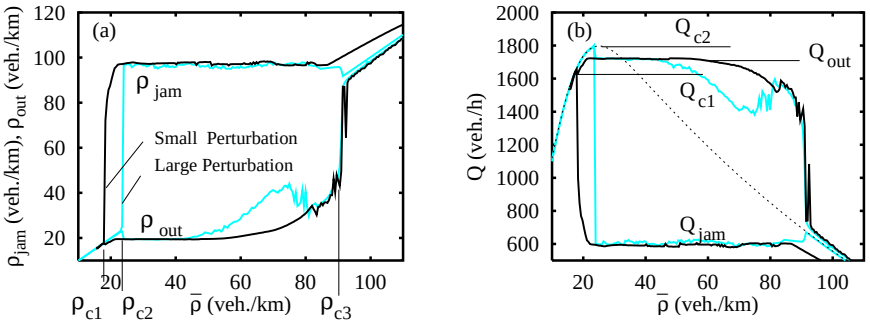

Fig. 2. Stability diagram of homogeneous traffic (for "car" parameters) in a closed system as a function of the homogeneous density $\overline{\rho}$ for small (grey) and large (black) initial perturbations of the density. In plot (a), the upper two lines display the density inside of density clusters after a stationary state has been reached. The lower two lines represent the density between the clusters. Plot (b) shows the corresponding flows and the equilibrium flow-density relation (dotted). The critical densities ρ_{ci} and flows Q_{ci} are discussed in the main text.

jams. Figure 2(b) shows the stability diagram for the flows. In particular, we have $Q_{\rm c1} < Q_{\rm out} < Q_{\rm c2}$, where $Q_{ci} = Q_{\rm e}(\rho_{ci})$, i.e., the outflow from congested traffic is metastable, while in the GKT, $Q_{\rm out} \approx Q_{\rm c2}$ is only marginally stable.

In *open* systems, a third type of stability becomes relevant. Traffic is *convectively* stable, if, after a sufficiently long time, all perturbations are convected out of the system. Both in the macroscopic models and in the IDM, there is a considerable density region $\rho_{\rm cv} \leq \overline{\rho} \leq \rho_{\rm c3}$, where traffic is linearly unstable but convectively stable.

2.4 Calibration

The *fundamental relations* of homogeneous traffic are calibrated with v_0 (low density), δ (transition region), T (high density), and s_0 and s_1 (jammed traffic). The *stability behavior* of traffic in the IDM model is determined mainly by the model parameters a, b, and T. The density in and the outflow from traffic jams are also influenced by s_0 and s_1. Since the accelerations a and b do not influence the fundamental diagram, the model can be calibrated essentially independently with respect to traffic flows and stability. As in the GKT model, traffic becomes more unstable for decreasing a (which corresponds to an increased acceleration time $\tau = v_0/a$), and for decreasing T (corresponding to reduced safe time headways). Furthermore, the instability increases with growing b. This is also plausible, because an increased desired deceleration b corresponds to a less anticipative or less defensive braking behavior.

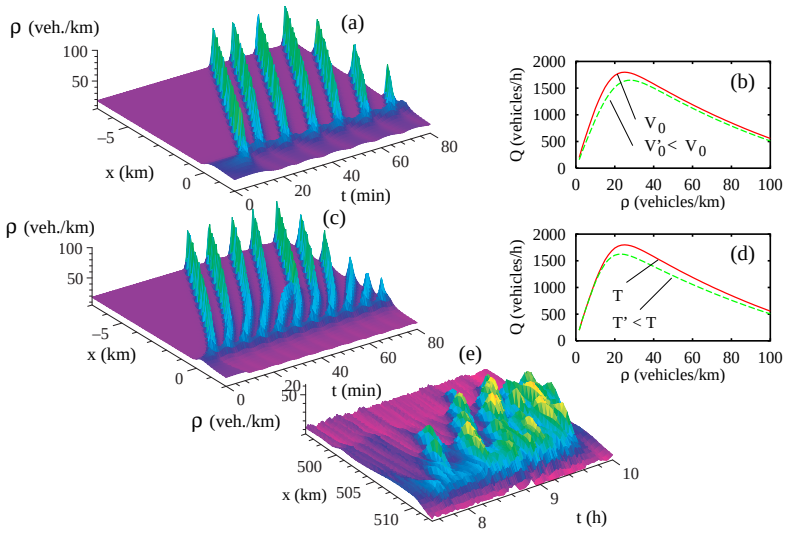

Fig. 3. Traffic breakdowns at differently implemented bottlenecks. (a) IDM simulation of the spatio-temporal density (inflow $Q_{\text{in}} = 1670$ vehicles/h) for a bottleneck corresponding to a decrease of v_0 in the downstream region. The density is derived from the microscopic distance s via relation (5) and a subsequent linear interpolation. (b) Related equilibrium flows upstream and downstream. (c), (d) Bottleneck corresponding to an increase of the safe time headway T. (e) Density obtained from 1-min detector data of the German freeway A9-South on Oct. 29, 1998. The traffic breakdown takes place upstream of the intersection "Neufahrn" at $x = 512$ km.

3 Microscopic Implementation of Bottlenecks

In *macroscopic* simulations, a natural implementation of road inhomogeneities is given by on- and off- ramps, which appear as a source term in the continuity equation for the density. An explicit *microscopic* modelling of ramps, however, would require a multi-lane model with explicit simulation of lane changes. In order to avoid the associated complications, one can either apply the micro-macro link and simulate the ramp section macroscopically [19], or introduce *flow-conserving* inhomogeneities by making one or more model parameters dependent on the location x of the road. Suitable parameters for the IDM are v_0 or T [15]. Local parameter variations act as a bottleneck, if the outflow Q'_{out} from congested traffic in the downstream section is reduced with respect to the outflow Q_{out} in the upstream section. This requires a reduced desired velocity $v'_0 < v_0$ or increased time headway $T' > T$, or both. Figure 3(a) shows a traffic breakdown induced by a linear decrease of the desired velocity from $v_0 = 120$ km/h for $x \le -L/2$ to $v'_0 = 95$ km/h for $x \ge L/2$, while Fig. 3(c) shows the same effect for an increase of the safe time headway from $T = 1.2$ s to $T' = 1.45$ s ($L = 200$ m). Both flow-conserving bottlenecks result in a similar traffic dynamics which, however, depends strongly on the amplitude of the parameter variation. Qualitatively

the same dynamics is observed in real traffic data [Fig. 3(e)] and in macroscopic models including on-ramps with a ramp flow of $Q_{\rm rmp} = Q_{\rm out} - Q'_{\rm out}$. This suggests to define a general "bottleneck strength" δQ by

$$\delta Q := Q_{\rm rmp} + Q_{\rm out} - Q'_{\rm out}. \tag{6}$$

In particular, we have $\delta Q = Q_{\rm rmp}$ for on-ramp bottlenecks, and $\delta Q = Q_{\rm out} - Q'_{\rm out}$ for flow-conserving bottlenecks. In the following, we will vary v_0. The regions with locally decreased desired velocity can be interpreted as sections with uphill gradients (which reduce the maximum velocities of vehicles).

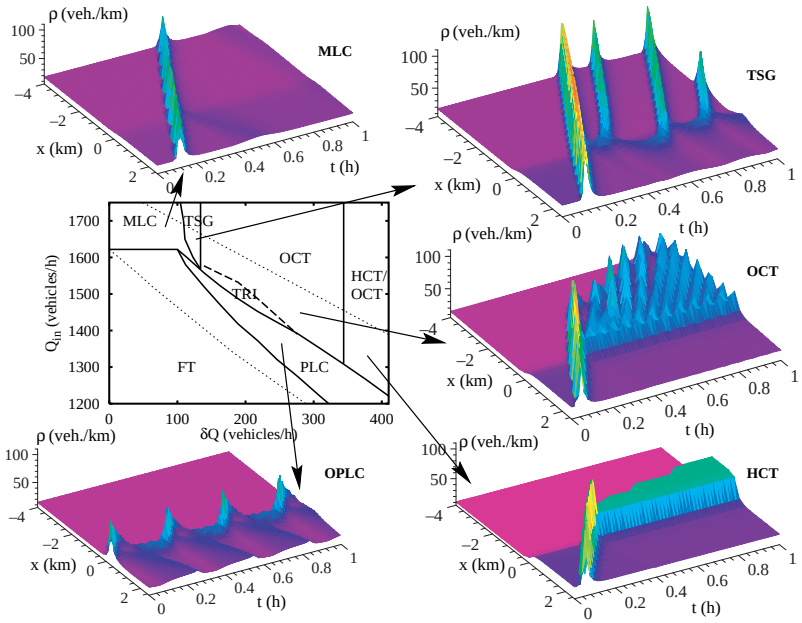

Fig. 4. Phase diagram of congested traffic states and corresponding spatio-temporal density plots as simulated with the IDM. The control parameters are the inflow $Q_{\rm in}$ and the bottleneck strength δQ, which increases with $(v_0 - v'_0)$. The traffic states FT, HCT, OCT, TSG, MLC, and (O)PLC are explained in the main text. "TRI" indicates a tristable region.

4 Phase Diagram of Congested Traffic

In contrast to *closed* systems, in which the long-term behavior and stability is essentially determined by the average traffic density, the dynamics of *open* systems is controlled by the inflow $Q_{\rm in}$. Furthermore, traffic congestions depend on road inhomogeneities and, because of hysteresis effects, on the history of previous perturbations. For a given history, the traffic states can

be summarized by a phase diagram spanned by $Q_{\rm in}$ and δQ. Figure 4 shows the IDM phase diagram for traffic states that develop after a single density cluster crosses the inhomogeneity. Depending on $Q_{\rm in}$ and δQ, the initial perturbation (i) dissipates, resulting in free traffic (FT), (ii) travels through the inhomogeneity as a moving localized cluster (MLC) and neither dissipates nor triggers new breakdowns, (iii) triggers a traffic breakdown to a pinned localized cluster (PLC), which remains localized near the inhomogeneity for all times and either is stationary, cf. Fig. 5(a) for $t < 0.2$ h, or oscillatory (OPLC). (iv) Finally, the initial perturbation can induce extended congested traffic (CT), whose downstream boundaries are fixed at the inhomogeneity, while the upstream front propagates further upstream in the course of time. This kind of congested traffic can be homogeneous (HCT), oscillatory (OCT), or consist of triggered stop-and-go waves (TSG). In contrast to OCT, where there is permanently congested traffic at the inhomogeneity ("pinch region" [13,15]), the TSG state is characterized by a series of isolated density clusters, each of which triggers a new cluster as it passes the inhomogeneity.

4.1 Boundaries between and Coexistence of Traffic States

Simulations show that the outflow $\tilde{Q}_{\rm out}$ from the nearly stationary downstream fronts of OCT and HCT satisfies $\tilde{Q}_{\rm out} \leq Q'_{\rm out}$, where $Q'_{\rm out}$ is the outflow from clusters in homogeneous systems for the downstream model parameters. If the bottleneck is not too strong, we have $\tilde{Q}_{\rm out} \approx Q'_{\rm out}$. Then, for all types of bottlenecks, the congested traffic flow is given by $Q_{\rm cong} = \tilde{Q}_{\rm out} - Q_{\rm rmp} \approx Q'_{\rm out} - Q_{\rm rmp}$, or

$$Q_{\rm cong} \approx Q_{\rm out} - \delta Q. \tag{7}$$

Extended congested traffic (CT) only persists, if the inflow exceeds the congested traffic flow. Otherwise, it dissolves to PLC. This gives the boundary

$$\text{CT} \rightarrow \text{PLC} : \delta Q \approx Q_{\rm out} - Q_{\rm in}. \tag{8}$$

If congested traffic flow is *convectively* unstable, the resulting oscillations lead to TSG or OCT. If it is *linearly* stable, $Q_{\rm cong} < Q_{\rm c3}$, we have HCT. If it is convectively stable, but linearly unstable, $Q_{\rm cong} \in [Q_{\rm c3}, Q_{\rm cv}]$, one has a spatial *coexistence* of states with HCT near the bottleneck and OCT further upstream [15] (Fig. 5), which is frequently found in empirical data of congested traffic. In the IDM, this frequent occurrence is reflected by the wide range of flows falling into this regime. For the "car" parameters, we have $Q_{\rm c3} = 600$ vehicles/h and $Q_{\rm cv} = 1340$ vehicles/h.

4.2 Multistability

In general, the local phase transitions between free traffic, pinned localized states, and extended congested states are hysteretic. In the regions between

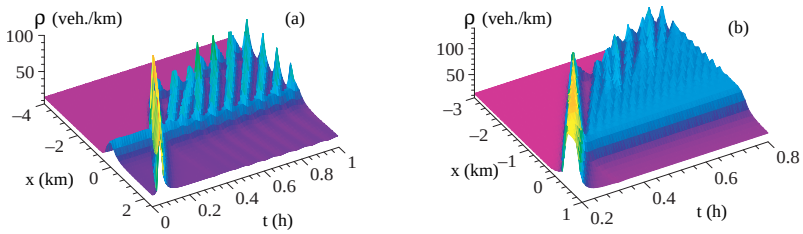

Fig. 5. (a) Transition from PLC to OCT in the tristable region ($Q_{\text{in}} = 1480$ vehicles/h, $v_0' = 24$ m/s corresponding to $\delta Q = 220$ vehicles/h), triggered by a large perturbation. (b) Spatial coexistence of HCT and OCT for $Q_{\text{in}} = 1350$ vehicles/h and $v_0' = 16$ m/s corresponding to $\delta Q = 400$ vehicles/h.

the two dotted lines of the phase diagram in Fig. 4, both, free and congested traffic is possible, depending on the previous history. In particular, for all five indicated phase points (but not for the simulations of Fig. 3), free traffic would persist without the downstream perturbation. In contrast, the transitions PLC-OPLC, and HCT-OCT-TSG seem to be non-hysteretic, i.e., the type of pinned localized cluster or of extended congested traffic, is uniquely determined by Q_{in} and δQ.

In a small subset of the metastable region, labelled "TRI" in Fig. 4, we even found *tristability* between FT, PLC, and OCT. We obtained qualitatively the same also for the GKT model, and it has been found for the KKL model with OPLC instead of PLC for the pinned localized state [18]. Figure 5(a) shows that a single moving localized cluster passing the inhomogeneity triggers a transition from PLC to OCT. Starting with free traffic, the same perturbation would trigger OCT as well, while we never found reverse transitions OCT → PLC or OCT → FT (without a reduction of the inflow). That is, FT and PLC are metastable in the tristable region, while OCT is stable.

4.3 Pinch Effect and Merging of Clusters

Careful investigations of traffic data related to OCT states [13] showed two phenomena: (i) In a narrow region near the inhomogeneity, there is nearly stationary congested traffic ("pinch region"), whereas further upstream, oscillations lead to temporarily lower traffic densities. (ii) While propagating upstream, the oscillations grow and merge to a few large-amplitude density clusters with free traffic in between. Detector data of other freeways, however, show this pinch effect without mergers, cf. Fig. 3(e). Simulating the IDM with the "car" parameters leads to very few mergers, cf. Figs. 3(c) and 4. For other parameters, however, the IDM reproduces mergers ending up with stop-and-go traffic [15]. A possible explanation is the *"starvation effect"*: For the parameters chosen in this article, the outflow Q_{out} from density clusters is in the middle of the metastable region [Fig. 2(b)], so medium-sized and large density clusters persist. For the parameters of Ref. [15], however, the outflow

from density clusters satisfies $Q_{\rm out} \approx Q_{\rm c1}$, so only large-amplitude clusters survive, while all others dissipate.

5 Multi-Species Single-Lane Traffic

In this section, we assume heterogeneous single-lane traffic consisting of 70% "cars" and 30% "trucks", where the latter are characterized by a lower desired velocity, lower accelerations, and a larger safe time headway compared to cars (Table 1). Again, we simulate a traffic breakdown to HCT at a flow-conserving inhomogeneity, where the desired velocity of cars is reduced from 120 km/h to 65 km/h, and that of trucks from 80 km/h to 36 km/h. (Similar results are found for less drastic increases of T.) To compare the result with real traffic data, we implement "virtual" detectors at several fixed locations. The detectors record passage times and velocities of each vehicle

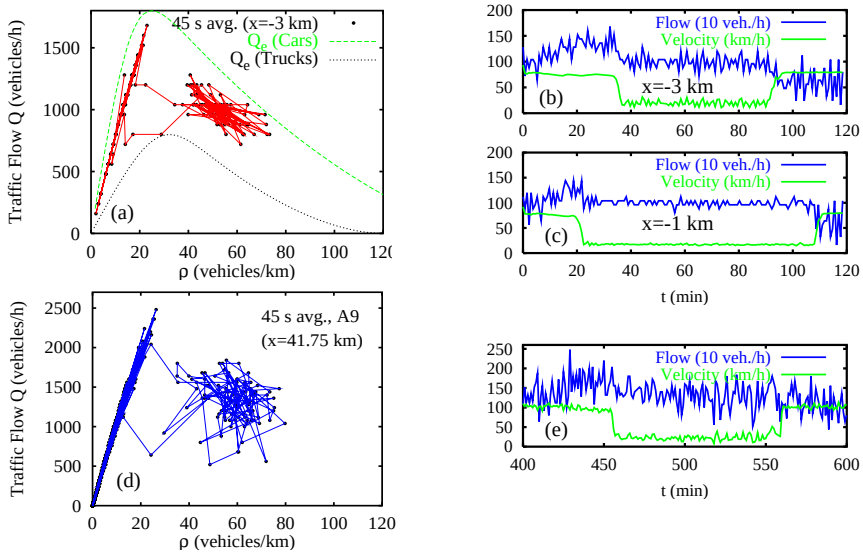

Fig. 6. (a) Flow-density diagram and (b)-(c) time series of single-lane heterogeneous traffic. (d)-(e) Empirical data of extended congested traffic on the Dutch freeway A9.

to determine the macroscopic flow $Q = n_\tau/\tau$ (n_τ is the number of passing vehicles in the averaging interval $\tau = 45$ s), the arithmetic velocity average V, and the density $\rho = Q/V$. Figure 6 shows the resulting fundamental diagram 3 km upstream of the bottleneck, and time series of Q and V at three upstream locations. For comparison, Fig. 6(d) and (e) show 45 s averages of *real* single-vehicle data of the Dutch freeway A9 from Haarlem to Amsterdam on October 14, 1994. The detector is about 0.7 km upstream of the on-ramp

causing the traffic breakdown. The simulated and real traffic data agree qualitatively, in particular in the following respects: (i) There is a wide scattering of flow-density data in the congested regime (looking like an anisotropic two-dimensional random walk), while the data occupy a nearly one-dimensional region in the free regime. (ii) The distribution of flow-density data shows the typical inverse-λ form with a distinct gap between free and congested traffic data. (iii) During the breakdown, the velocity drops to 10-20 km/h, while the flow is reduced by only about 20 %. (iv) In all regions, the relative fluctuations of the velocity are smaller than those of the flow. Near the bottleneck, the fluctuations of congested traffic flow are much smaller than those of free traffic, while further upstream, the fluctuations grow.

Notice that the fluctuations of the simulated data come essentially from the different vehicle types and not from deterministic instabilities. Macroscopically, the situation of Fig. 6 corresponds to a spatial coexistence of HCT and OCT. (For a pure OCT or TSG state, there would be no gap between the flow-density data of free and congested traffic, both in real traffic data and in simulations.)

6 Discussion

Although there are also other proposals for an explanation of the various transitions between free traffic, congested traffic, and stop-and-go waves [13], we see the following advantages of our approach: The transitions result *naturally* from a model for traffic flow on *homogeneous* roads, just by adding speed limits (like above), source terms (in case of on-ramp flows) [16], or other kinds of inhomogeneities, which are *known* to exist. The implementation of these inhomogeneities is *straightforward,* without the requirement of additional refined model ingredients. Moreover, analogous to the other parameters of the model, the inhomogeneities are easily measurable quantities. There is no model ingredient, which could not be relatively easily be verified or falsified by empirical studies. Furthermore, *empirical results* confirming the existence of a phase diagram are already available [9]. Finally, we think that the simulated traffic states related to inhomogeneities of the road arise *so* naturally, that any explanation of empirical data must take these states into account. Our simulations show that, simply by assuming a mixture of different vehicle types, one can reproduce the observed scattering of flow-density data by a *deterministic* model having a *unique* equilibrium relation. The same has also been found for a macroscopic model [20]. Generalizations to multi-lane traffic result in an even better agreement with empirical findings, e.g., a larger scattering of "virtual" detector data and flow-stabilizing effects of speed limits [21,22]. To us, the most interesting open question is which kind of observable phenomena are produced by the heterogeneity of driver-vehicle units *in addition* to the scattering of traffic data [23].

References

1. Reuschel, A.: Fahrzeugbewegungen in der Kolonne. *Österreichisches Ingenieur-Archiv* **4** (1950) 193–215.
2. Newell, G. F.: Nonlinear effects in the dynamics of car following. Operations Research **9** (1961) 209ff.
3. Bando, M., Hasebe, K., Nakayama, A., Shibata, A., and Sugiyama, Y.: Dynamical model of traffic congestion and numerical simulation. *Phys. Rev. E* **51** (1995) 1035–1042.
4. Gipps, P. G. A behavioural car-following model for computer simulation. *Transportation Research B* **15** (1981) 105–111.
5. Krauß, S.: *Microscopic Modelling of Traffic Flow* (DLR, Cologne, 1998), FB 98-08.
6. Helbing, D. and Tilch, B.: Generalized force model of traffic dynamics. *Phys. Rev. E* **58** (1998) 133–138.
7. Wiedemann, R.: *Simulation des Straßenverkehrsflusses* (Institut für Verkehrswesen, Universität Karlsruhe, 1974).
8. See internet page `http://hippo.mit.edu/products/mitsim/main.html`.
9. Lee, H. Y., Lee, H. W., and Kim, D.: Empirical phase diagram of congested traffic flow. Preprint cond-mat/9905292.
10. Kerner, B. S. and Rehborn, H.: Experimental properties of complexity in traffic flow. *Phys. Rev. E* **53** (1996) R4275–R4278.
11. Treiterer, J. and Myers, J. A.: The hysteresis phenomenon in traffic flow. In Proc. 6th Int. Symp. on Transportation and Traffic Theory, D. J. Buckley, ed., (Elsevier, New York, 1974), pp. 13ff.
12. Daganzo, C. F., Cassidy, M. J., and Bertini, R. L.: Some traffic features at freeway bottlenecks. *Transportation Research B* **33** (1999) 25–42.
13. Kerner, B. S.: The physics of traffic. *Physics World* (Aug./1999), 25–30.
14. Kerner, B. S. and Konhäuser, P.: Structure and parameters of clusters in traffic flow. *Phys. Rev. E* **50** (1994) 54–83.
15. Treiber, M. and Helbing, D.: Explanation of observed features of self-organization in traffic flow. Preprint cond-mat/9901239.
16. Helbing, D., Hennecke, A., and Treiber, M.: Phase diagram of traffic states in the presence of inhomogeneities. *Phys. Rev. Lett.* **82** (1999) 4360–4363.
17. Treiber, M., Hennecke, A., and Helbing, D.: Derivation, properties, and simulation of a gas-kinetic-based, non-local traffic model. *Phys. Rev. E* **59** (1999) 239–253.
18. Lee, H. Y., Lee, H. W., and Kim, D.: Origin of synchronized traffic flow on highways and its dynamic phase transition. *Phys. Rev. Lett.* **81** (1998) 1130–1133.
19. Hennecke, A., Treiber, M., and Helbing, D.: Macroscopic simulation of open systems and micro-macro link. In this volume.
20. Treiber, M. and Helbing, D.: Macroscopic simulation of widely scattered synchronized traffic states. *J. Phys. A: Math. Gen.* **32** (1999) L17–L23.
21. Interactive simulations of the multi-lane IDM are available at `http://www.uni-stuttgart.de/treiber/MicroApplet/`.
22. Sollacher, R. and Lenz, H.: Nonlinear control of stop-and-go traffic. In this volume.
23. Helbing, D. and Huberman, B. A.: Coherent moving states in highway traffic. *Nature* **396** (1998) 738–740.